JGR Oceans

RESEARCH ARTICLE
10.1029/2023JC020504

Seasonal Predictability of Bottom Temperatures Along the North American West Coast

Tongtong Xu[1,2], Matthew Newman[2], Michael A. Alexander[2], and Antonietta Capotondi[1,2]

[1]CIRES, University of Colorado, Boulder, CO, USA, [2]NOAA Physical Sciences Laboratory, Boulder, CO, USA

Key Points:

- Skill of Bottom Temperature (BT) forecasts along the North American West Coast by a Linear Inverse Model exceeds damped persistence
- Elevated BT forecast skill is linked to El Niño-Southern Oscillation, with a delayed response along the coast relative to the tropical Pacific
- BT predictability is higher at locations with ~50–150 m bathymetric depth, and in Canadian waters

Supporting Information:

Supporting Information may be found in the online version of this article.

Correspondence to:

T. Xu,
tongtong.xu@noaa.gov

Citation:

Xu, T., Newman, M., Alexander, M. A., & Capotondi, A. (2024). Seasonal predictability of bottom temperatures along the North American West Coast. *Journal of Geophysical Research: Oceans*, *129*, e2023JC020504. https://doi.org/10.1029/2023JC020504

Received 21 SEP 2023
Accepted 2 SEP 2024

Author Contributions:

Conceptualization: Tongtong Xu, Matthew Newman, Michael A. Alexander, Antonietta Capotondi
Data curation: Tongtong Xu
Formal analysis: Tongtong Xu
Funding acquisition: Matthew Newman
Investigation: Tongtong Xu
Methodology: Tongtong Xu, Matthew Newman
Supervision: Matthew Newman, Michael A. Alexander, Antonietta Capotondi
Validation: Tongtong Xu
Visualization: Tongtong Xu
Writing – original draft: Tongtong Xu

Abstract Bottom Temperature anomalies (BTA) along the North American West Coast strongly influence benthic and demersal marine species. However, to date seasonal BTA forecast efforts have been limited and sources of BTA predictability largely undiagnosed. Here, an empirical model called a Linear Inverse Model (LIM), constructed from a high-resolution ocean reanalysis, is developed to predict North American West Coast BTAs and diagnose sources of predictive skill. The LIM is considerably more skillful than damped persistence, particularly in winter, with anomaly correlation (AC) skill values of 0.6 at 6-month lead. Analysis of the LIM's dynamics shows that elevated BTA forecast skill is linked to developing El Niño-Southern Oscillation (ENSO) events, driving predicted BTA responses whose peaks occur at longer leads with increasing latitude. Weaker ENSO-related signals in the northern coastal region still yield high BTA skill because noise there is also weaker. Likewise, the LIM's forecast signal-to-noise ratio is highest for bathymetry depths of ~50–150 m, maximizing forecast skill there. Together, these predictive components lead to "forecasts of opportunity" when LIM anticipates especially high prediction skill. For the top 20% of events identified by the LIM as the forecasts of opportunity, 6-month lead BTA hindcasts have AC skill averaging 0.7, while the remaining 80% hindcasts have mean skill of only 0.4, suggesting that the LIM can leverage ENSO-related predictability of BTA to produce skillful forecasts.

Plain Language Summary Along the North American West Coast, ocean bottom conditions such as Bottom Temperatures (BT) can directly affect the ecosystem of marine species living at and near the sea floor. Unfortunately, long-term subsurface observations with fine spatial resolution in this region have been few, and it is not yet well understood whether prediction systems could make seasonal forecasts of BT with enough skill to be useful. In this study, we construct a statistical prediction model, called a Linear Inverse Model (LIM), to predict BTs along the North American West Coast and identify when, where and how our predictions of BTs may be especially good. We find that the LIM can make predictions that substantially improve upon assuming that ocean conditions continue unchanged. Furthermore, we find that much of the LIM skill occurs when predicting winter conditions and is linked to El Niño-Southern Oscillation (ENSO), the dominant predictable climate phenomenon on year-to-year time scales. Moreover, the LIM can use its ability to predict ENSO to also predict which of its BT forecasts will be most skillful. Its BT prediction is best for locations where the ocean bottom is around 50–150 m deep, which may be related to different depth-dependent processes influencing ocean characteristics.

1. Introduction

The coastal ocean along the North American West Coast is an essential ecosystem habitat, which naturally supplies numerous nutrients critical for the living of marine species, contributing to high proportion of commercial fish yield (e.g., Capone & Hutchins, 2013; Stock et al., 2015). Among relevant physical drivers, ocean temperature has been identified as a leading factor affecting the physiological processes of aquatic organisms and species (e.g., Drinkwater et al., 2010; Ottersen et al., 2010; Sampaio & Rosa, 2020). Thus, skillful forecasts of ocean temperature are crucial for reliably predicting future ecosystem fluctuations and for providing guidance on mitigation strategies.

Predictions of ocean temperatures have mainly focused at the surface, which is more easily measured and observed than the deeper ocean. Sea Surface Temperature (SST) seasonal forecasts along the North American West Coast have shown skill (e.g., Hervieux et al., 2019; Jacox et al., 2019; Stock et al., 2015), apparently associated with local and remote effects of El Niño-Southern Oscillation (ENSO) (e.g., Capotondi, Sardeshmukh, et al., 2019; Jacox et al., 2019; Wen et al., 2012). During ENSO development, equatorial Kelvin waves propagate

Writing – review & editing:
Tongtong Xu, Matthew Newman, Michael A. Alexander, Antonietta Capotondi

eastward along the equator, and then continue poleward along the coast as coastally-trapped Kelvin waves, inducing thermocline variability (e.g., Amaya et al., 2022; Engida et al., 2016; Jacox et al., 2015; Ray et al., 2020). These coastally-trapped waves have amplitude and offshore scale that decrease with latitude (e.g., Frischknecht et al., 2015; Gómez-Valdivia et al., 2017; Hermann et al., 2009), so that they may be more impactful in the lower-latitude coastal waters. At higher latitudes, changes in atmospheric circulation associated with ENSO atmospheric teleconnections may play a greater role. These atmospheric circulation changes involve a deepening and eastward displacement of the Aleutian Low, causing variations in the alongshore winds and coastal upwelling (e.g., Ding et al., 2021; Hermann et al., 2009; Jacox et al., 2015), and usually follow the ENSO peak phase by a few months (e.g., Alexander et al., 2002; Deser & Blackmon, 1995; Liu & Alexander, 2007).

On the other hand, ocean bottom conditions can directly affect the abundance and distribution of benthic and demersal marine species (e.g., Barbeaux et al., 2020; Keller et al., 2015; Norton et al., 2020), so forecasting Bottom Temperatures (BT) along the continental shelf is also very important. Recent studies (Alexander et al., 2023; Amaya, Jacox, et al., 2023) have shown that BTs are highly correlated with SSTs in relatively shallow regions, where the mixed layer can extend close to the sea floor, suggesting that in those regions, mechanisms contributing to SST variability and predictability may also contribute to the predictability of BT. In addition to mixed layer dynamics, vertical movements of the thermocline due, for example, to coastal wave propagation or variability of coastal upwelling, can also influence both SSTs and BTs in those regions where the ocean depth is comparable to thermocline depth. Deep locations below the thermocline, on the other hand, may experience variability that is unrelated to SST, but is more affected by subsurface ocean currents (e.g., the California undercurrent) and their interactions with the local bathymetry (e.g., Breaker, 2019; Kurczyn et al., 2019; Ray et al., 2020).

Until now, only a few studies have examined BT forecasts and the sources of BT predictability. The main tools for seasonal predictions are climate models. Yet the resolution of the current generation of climate models is relatively coarse, and unable to sufficiently capture the shelf-scale dynamics and coastal processes (Stock et al., 2011). This has led to efforts using dynamical downscaling techniques (see reviews by Jacox et al., 2020), which typically involve the use of a regional ocean model forced at the ocean surface and lateral boundaries by the output of a global model. Studies that used dynamical downscaling to predict BT showed differences in skill in different regions. For example, the dynamical downscaling conducted by JISAO's Seasonal Coastal Ocean Prediction of the Ecosystem (J-SCOPE) (Siedlecki et al., 2016), for Washington and Oregon coastal waters, indicated that BTs are more realistically simulated than SSTs and that BT forecasts are more skillful at mid-shelf locations than at shallower sites. On the other hand, another dynamical downscaling application in the Eastern Bering Sea Shelf (Kearney et al., 2021), a region strongly affected by seasonal sea ice cover, suggested that the BT forecast skill there is only marginally better than persistence, and that sea ice is a prediction barrier. For the California Current System, dynamically downscaled forecasts exhibit greater persistence and better forecasts of BT than SST; the skill of both is mainly associated with ENSO teleconnections (Jacox et al., 2023).

While these examples demonstrate that dynamical downscaling approaches might be used for high-resolution BT forecasts, such approaches can also be computationally very expensive, and even more so for probabilistic forecasts where many ensemble members are needed. In addition, downscaled forecasts may inherit the biases of the global forecast models that provide the surface forcing and lateral boundary conditions, possibly introducing errors in the predicted fields (Capotondi, Jacox, et al., 2019; Jacox et al., 2020). These issues with dynamical downscaling make alternative statistical approaches very attractive, especially with the recent release of GLORYS12v1 global Mercator Ocean and sea ice reanalysis (Jean-Michel et al., 2021), an eddy-resolving global ocean product with sufficient horizontal resolution (1/12°, ∼9 km) to reasonably resolve the North American coastal environment (Alexander et al., 2023; Amaya, Jacox, et al., 2023; Cai et al., 2021; Chi et al., 2018). For example, this high-resolution data set was used to train a set of simple linear regression models using indices (such as Gulf Stream indices) to predict BT along the Northeast U.S. Continental Shelf, demonstrating that oceanic advection, from both the Labrador Current and the Gulf Stream, contributes to enhance BT hindcast skill above persistence (Chen et al., 2021). Additionally, Long et al. (2023) developed a multivariate linear regression statistical downscaling approach trained using this data set to produce high-resolution U.S. coastal sea level forecasts from coarser seasonal climate predictions. These results suggest that the GLORYS12v1 data set could be used to develop empirical techniques at the resolution needed to make coastal BT forecasts.

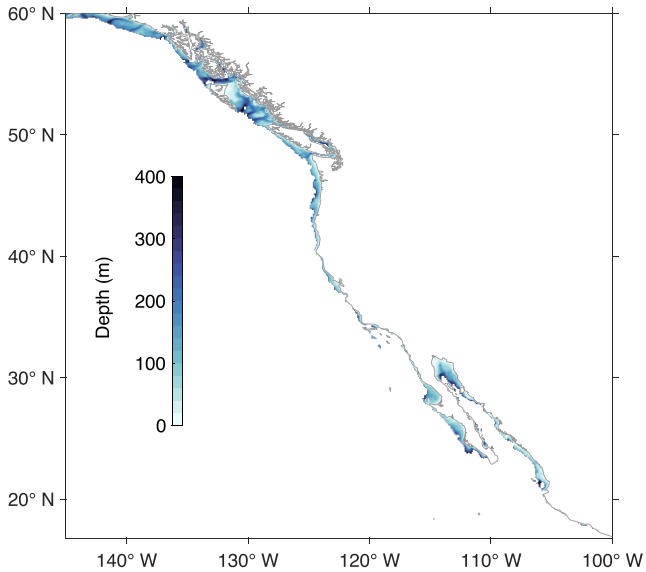

Figure 1. Bathymetry depth (m) along the North American West Coast.

A multivariate empirical dynamical approach that has proven useful in climate prediction is the Linear Inverse Model (LIM; Penland & Sardeshmukh, 1995). Numerous studies have shown that LIMs realistically capture the seasonal evolution of surface anomalies in the Pacific sector (e.g., Alexander et al., 2008; Capotondi et al., 2022; Lou et al., 2021; Xu et al., 2021; Zhao et al., 2021), producing SST forecasts with skill comparable to operational forecast models (e.g., Newman & Sardeshmukh, 2017; Shin & Newman, 2021). Additionally, the LIM can estimate potential predictability, of both itself and other forecast models (e.g., Newman & Sardeshmukh, 2017), including determining—in advance—forecasts with potentially higher prediction skill, sometimes called "forecasts of opportunity" (e.g., Albers & Newman, 2019; Mariotti et al., 2020).

Motivated by these studies, we construct a LIM for the Pacific basin, to forecast BTs along the North American West Coast on seasonal timescales, trained using the GLORYS12v1 data set. By applying the LIM to BTs, we aim to answer the following questions: (a) how well can we forecast BTs in this region, and (b) can we identify key mechanisms or conditions conducive to skillful BT forecasts? The paper is organized as follows. In Section 2, we describe the ocean reanalysis state variables and their preprocessing, followed by an introduction of the LIM methodology and its application to the identification of "forecasts of opportunity," within the LIM framework. In Section 3, we present our hindcast results, including the seasonal and bathymetric depth dependence of the hindcast skill, and highlight how the BT predictability is linked to ENSO. A summary is described in Section 4.

2. Data and Methods

2.1. Data

We use monthly BTs, SSTs, and Sea Surface Heights (SSHs) over the years 1993–2019, obtained from the GLORYS12v1 ocean reanalysis (Jean-Michel et al., 2021) provided by the Copernicus Marine Environmental Monitoring Service. This data set assimilates along-track satellite altimetry for SSH, satellite SST, sea ice concentrations, and in situ profiles of temperature and salinity, including ARGO floats, from the Coriolis Ocean database ReAnalysis (CORA) data set (Szekely et al., 2019). We chose GLORYS12v1 for its reasonably good representation of the North American coastal environment (e.g., see Alexander et al., 2023; Amaya, Jacox, et al., 2023; Castillo-Trujillo et al., 2023; and references therein). We focus on BT along the North American West Coast, spanning 15°–60°N, 145° and 100°W, and for bottom depths to 400 m (Figure 1). Pacific basin SST and SSH (extending from 20°S to 60°N and from 100°E to 68°W) are incorporated for their potential contribution to BT forecasts. Anomalies of each field (BTA, SSTA, SSHA) are obtained by removing the seasonal mean climatology and subtracting the linear trend. While the long-term trend has evolved nonlinearly within some regions (Frankignoul et al., 2017; Xu et al., 2022), a linear estimate may be reasonable for the short period of 1993–2019.

2.2. Linear Inverse Model

A LIM assumes that the evolution of coarse-grained climate anomalies can be approximated by deterministic linear dynamics plus unpredictable (rapidly decorrelating) nonlinearities represented as stochastic white noise forcing, or:

$$\frac{d\mathbf{x}}{dt} = \mathbf{L}\mathbf{x} + \boldsymbol{\xi} \tag{1}$$

where $\mathbf{x}(t)$ is a climate anomaly state vector, $\mathbf{L}$ is a stable linear dynamical operator, $\boldsymbol{\xi}(t)$ is temporally white noise (which can have spatial coherence determined from a balance relation), and t is time (Penland & Sardeshmukh, 1995). $\mathbf{L}$ is determined from the observed simultaneous and lagged covariances of $\mathbf{x}(t)$, as described in Penland and Sardeshmukh (1995) and Newman, Sardeshmukh, et al. (2003):

$$\mathbf{L} = \tau_0^{-1} \ln\left(\mathbf{C}(\tau_0)\,\mathbf{C}(0)^{-1}\right) \tag{2}$$

in which $\mathbf{C}(0) = \langle \mathbf{x}(t)\mathbf{x}(t)^{\mathrm{T}} \rangle$ is the auto-covariance matrix, $\mathbf{C}(\tau_0) = \langle \mathbf{x}(t+\tau_0)\mathbf{x}(t)^{\mathrm{T}} \rangle$ is the lag-τ_0 covariance, and τ_0 denotes the time lag between $\mathbf{x}(t)$ and $\mathbf{x}(t+\tau_0)$. Note that τ_0 is a training lag. If (Equation 1) is a reasonable representation of the climate dynamical evolution, the resulting $\mathbf{L}$ operator should be independent of the chosen τ_0, and capable of accurately reproducing lag-covariance statistics at lags longer than the training lag (Penland & Sardeshmukh, 1995). Here we chose $\tau_0 = 1$ month, following previous studies that have tested the suitability of such a training lag (e.g., Newman & Sardeshmukh, 2017; Shin & Newman, 2021; Xu et al., 2022).

Having obtained $\mathbf{L}$, ensemble-mean forecasts for any lead time τ are

$$\hat{\mathbf{x}}(t+\tau) = \exp(\mathbf{L}\tau)\,\mathbf{x}(t) \equiv \mathbf{G}(\tau)\,\mathbf{x}(t), \tag{3}$$

with expected forecast error variance determined by the diagonal of

$$\mathbf{E}(\tau) = \mathbf{C}(0) - \mathbf{G}(\tau)\,\mathbf{C}(0)\,\mathbf{G}(\tau)^{\mathrm{T}} \tag{4}$$

in which $\mathbf{E}(\tau)$ is the expected forecast error covariance matrix, and $\mathbf{G}(\tau) \equiv \exp(\mathbf{L}\tau)$ is the Green's function.

In our study, $\mathbf{x}(t)$ consists of coastal BTA, Pacific SSTA and SSHA. To reduce dimensionality, anomalies of each field were first projected on their Empirical Orthogonal Functions (EOFs) to obtain the associated time evolving amplitudes, that is, Principal Components (PCs). $\mathbf{x}(t)$ is then constructed by a leading subset of PCs of each field. We retain the leading 15/9/8 PCs of BTA/SSTA/SSHA, representing 84/54/39% of each field's variance. This combination of PCs is chosen to maximize the cross-validated prediction skill of BTA. Truncating to different numbers of PCs does not fundamentally change our results.

Following previous LIM studies (e.g., Breeden et al., 2022; Newman & Sardeshmukh, 2017; Shin & Newman, 2021), independent prediction skill is evaluated through ten-fold cross-validation. This is done by first dividing the data record into 10 subsamples with equivalent lengths. We compute the linear operator $\mathbf{L}$ from 90% of the data record (i.e., 9 subsamples). This $\mathbf{L}$ is then applied to the remaining 10% record (i.e., 1 subsample), which serve as initial conditions to obtain the subsequent 1–12 months forecast. This process is repeated 10 times to obtain retrospective forecasts (called "hindcasts") for each 10% record, which are then concatenated together into the hindcast time series over the full length of the data record. Hindcast skill is measured using local anomaly correlation between the hindcasts and their corresponding observed verifications (e.g., Albers & Newman, 2019; Siegert et al., 2017; Yang et al., 2021), and (in the Supporting Information S1) with the Mean Square Error (MSE) skill score (e.g., Murphy & Epstein, 1989; Newman & Sardeshmukh, 2017), another commonly used skill metric. MSE skill score quantifies the standardized error, defined as the square error between observations and forecasts, divided by the observed variance, which is also the square error between observations and the climatological anomaly forecast (i.e., zero). Further details, including how the significance testing was conducted, are also in the Supporting Information S1.

2.3. Diagnosing LIM Predictability

In some sense, predictability (or potential forecast skill) represents a tradeoff between the deterministic (predictable) signal and the inherent uncertainty induced by unpredictable noise (Lorenz, 1963; Scaife & Smith, 2018). It therefore may be assessed using a forecast signal-to-noise ratio, which in the LIM is easily determined using (Equations 3 and 4) from the ratio of the forecast variance and the expected error variance. The expected LIM forecast skill (e.g., measured by anomaly correlation) is then a monotonic function of this ratio (Sardeshmukh et al., 2000).

Since forecast error variance from (Equation 4) depends only on lead time and not on the initial anomaly, case-to-case variations in expected LIM forecast skill are entirely determined by variations of forecast amplitude in (Equation 3) (Newman, Sardeshmukh, et al., 2003). Forecasts of opportunity may therefore be identified in advance by determining relatively small-amplitude initial conditions that undergo maximum anomaly amplification over

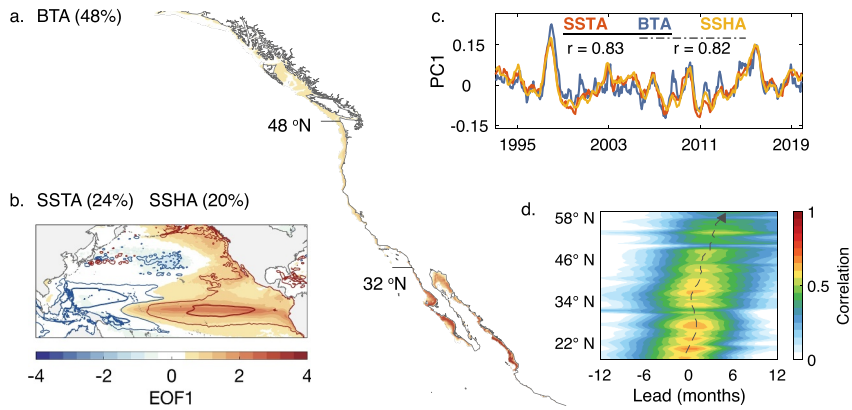

Figure 2. Dominant patterns of variability. The leading Empirical Orthogonal Function (EOF1) of (a) Bottom Temperature Anomaly (BTA), (b) Sea Surface Temperature Anomaly (SSTA; shading), and Sea Surface Height Anomaly (SSHA; contour; unit: 1). Contour is SSHA at values 2 (thin), 4 (thick) (positive: red; negative: blue). Percentage variance explained by each EOF1 is marked. (c) The corresponding Principal Component (PC1) of BTA (blue), SSTA (red), and SSHA (orange). Correlations between PC1 of different variables are indicated on top of panel (c). EOF1/PC1 of each field is separately normalized for display purpose. (d) Lead-lag correlation (x-axis) between SSTA PC1 and local BTA, derived for each grid point, averaged for every 0.6° latitudinal bin, and displayed as a function of latitude (y-axis). Positive (negative) leads denote SSTA PC1 preceding (following) local BTA. Dashed line is the peak correlation at each latitude.

some finite time interval τ (e.g., Breeden et al., 2020; Capotondi et al., 2022). Such "optimal precursors" are identified by the amplitude ratio γ^2 between an initial and a final state over the time interval τ, measured by

$$\gamma^2(\tau) = \frac{\mathbf{x}(t)^{\mathrm{T}}\mathbf{G}(\tau)^{\mathrm{T}}\mathbf{N}\mathbf{G}(\tau)\,\mathbf{x}(t)}{\mathbf{x}(t)^{\mathrm{T}}\mathbf{x}(t)} \tag{5}$$

where $\mathbf{N}$ is a matrix representing a final pattern or target variable of interest (Farrell, 1988). In this study, we use $\mathbf{N}$ to target BTA throughout the coastal domain, such that

$$\mathbf{N} = \begin{bmatrix} \mathbf{I} & \\ & 0 \end{bmatrix} \tag{6}$$

where $\mathbf{I}$ is the identity matrix, that is, only diagonal elements corresponding to BTA are 1 and all other elements are 0. This $\mathbf{N}$ is to maximize the ratio between the amplitude of the evolved BTA and the amplitude of the initial conditions, with the aim of identifying precursors leading to particularly skillful BTA predictions. The optimal precursor that subsequently leads to maximum BTA growth over a given time interval τ is simply the leading eigenvector of $\mathbf{G}(\tau)^{\mathrm{T}}\mathbf{N}\mathbf{G}(\tau)$.

3. Results

3.1. North American West Coast BTA Variability

Along the West Coast, BTA variability is dominated by a pattern with larger magnitude in the southern (Baja California) than in the northern parts of the domain, captured by the leading EOF of BTA (Figure 2a). The dominant patterns of Pacific SSTA and SSHA (EOFs shown in Figure 2b) are both typical of the mature phase of ENSO: large SSTA amplitude in the central and eastern Pacific, and an east-west SSH dipole indicative of a deeper (shallower) thermocline in the eastern Pacific and a shallower (deeper) thermocline in the western Pacific (e.g., Capotondi et al., 2020; Meinen & McPhaden, 2000). The time evolving amplitudes of the leading EOFs for each field (i.e., their PCs) are shown in Figure 2c. While each field's dominant pattern is determined separately, their PCs are highly correlated ($r = 0.8$), suggesting that BTA along the North American West Coast may be linked to ENSO variability in the tropical Pacific.

As ENSO may exhibit its influence along the coast with different lags, we may expect some lead-lag response between ENSO and BTA variability. Indeed, we find ENSO tends to lead BTA along the West Coast by a few

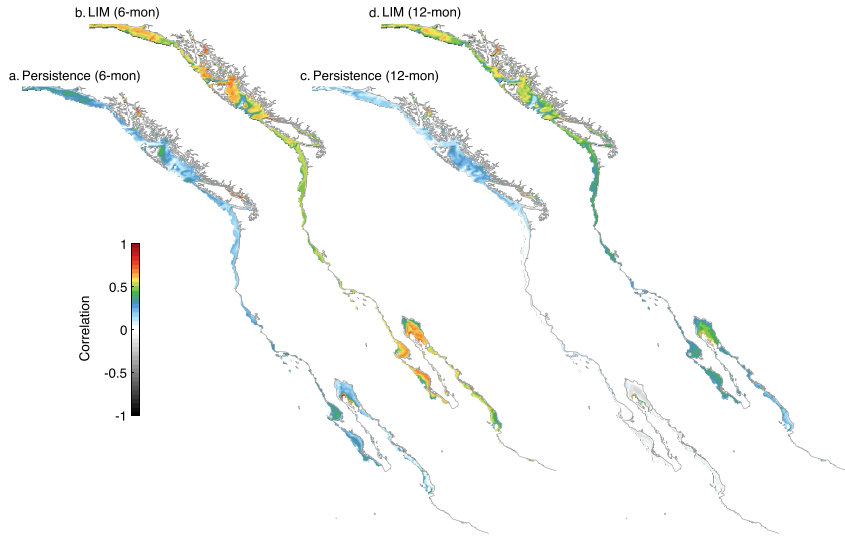

Figure 3. BTA hindcast skill (anomaly correlation) comparison between damped persistence and Linear Inverse Model (LIM). (a, c) Damped persistence for leads of (a) 6 and (c) 12 months, and (b, d) LIM hindcast skill for leads of (b) 6 and (d) 12 months.

months, illustrated by the lead-lag correlation between the leading SSTA PC and the BTA time series determined for each latitude along the coast (Figure 2d). BTA variations appear quasi-synchronous with ENSO in the southern part of the coastal domain, since BTA is maximally correlated there with the leading SSTA PC at about 0-month lag. Moving poleward, the correlation peaks at gradually longer lags (~5 months in the north), indicating a delayed response of the coastal BTA signal to ENSO. A similar delayed response has been found between SSTA in the California Current System and the tropical Pacific (e.g., Jacox et al., 2019).

3.2. Skillful Seasonal BTA Prediction

The potential link between BTA along the North American West Coast and ENSO motivates the construction of the Pacific LIM (Section 2.2) and its use for seasonal BTA prediction. Figure 3 compares the LIM's BTA hindcast skill to damped persistence, which gauges how much prediction skill is due to local memory alone, damped at a rate equal to the autocorrelation of BTA. Damped persistence is often used as a baseline for the prediction skill of many ocean variables (e.g., Amaya et al., 2022; Jacox et al., 2019; Long et al., 2021; Qiu et al., 2014). Evaluated in terms of local anomaly correlation, the 6-month-lead damped persistence skill (Figure 3a) is ~0.3 on average, and the 12-month-lead damped persistence skill (Figure 3c) is only ~0.1.

LIM hindcasts are significantly more skillful than damped persistence in most locations. Skill values are as high as ~0.6 for leads of 6 months in Canadian coastal waters and along Baja California (Figure 3b), and still ~0.6 at 12-month lead in Canadian waters (Figure 3d). Skill determined separately for southern, central, and northern sub-regions is shown as a function of verification month and lead time in Figure 4. For all three sub-regions (Figures 4a–4c), skill values are significant for LIM hindcasts verified during winter/spring, for lead times up to ~10–12 months. When verifying during summer/fall, LIM hindcast skill is generally lower than winter/spring, especially in the southern and central sub-regions. ENSO seasonality has been found to drive similar seasonal variations in skill for coastal SSTA, SSHA, BTA, and stratification forecasts (Jacox et al., 2019, 2023; Shin & Newman, 2021), and it may be similarly influencing LIM BTA hindcast skill.

There is also both a seasonal and latitudinal dependence to the locations and times when LIM prediction of BTA is relatively more skillful. In the southern sub-region, the LIM is significantly more skillful than damped persistence in the late fall and the early winter (Figure 4d). Moving poleward, the central sub-region shows significantly enhanced skill relative to damped persistence in late winter (Figure 4e) and the northern sub-region is improved in early spring (Figure 4f). This relatively high skill, moving northward from fall to winter to spring, suggests that the LIM dynamics capture the observed northward progression of the ENSO influence seen in Figure 2d. Similar results are seen with other skill metrics, including MSE skill score (cf. Figures S1 and S2 in Supporting

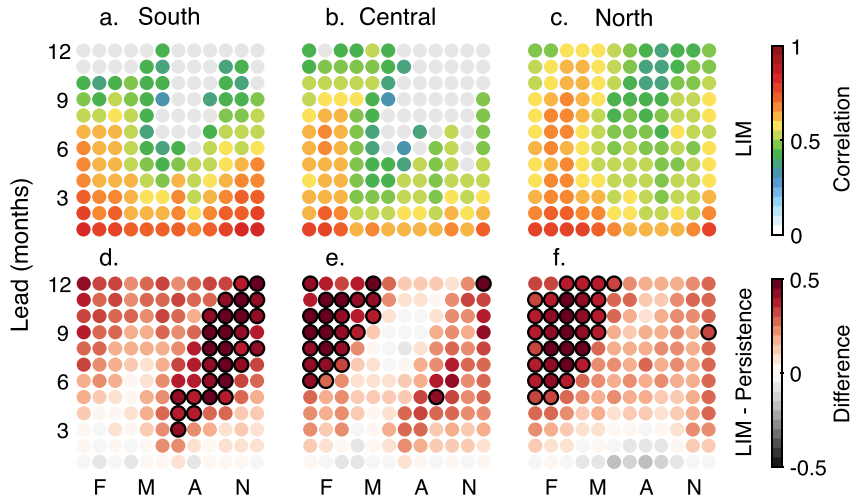

Figure 4. (a–c) LIM forecast skill at 1–12 months leads compared to (d–f) damped persistence, spatially averaged for (a, d) southern (south of 32°N), (b, e) central (32°N–48°N), and (c, f) northern (north of 48°N) sub-regions. (a–c) LIM hindcast skill, where color dots represent significant skill values (95% confidence level based on bootstrapping). (d–f) Difference between LIM and damped persistence skill, where dots with black outlines indicate LIM skill significantly above damped persistence (95% confidence level). Verification month is on the *x*-axis, lead time is on the *y*-axis. See Figure 2a for the geographic range of each sub-region.

Information S1 with Figures 3 and 4), which measures the mean amplitude rather than the mean phase of prediction errors. The consistency of our findings across both metrics reinforces the robustness of our results.

Given the northward progression of ENSO influences on BTA hindcasts, one may ask whether the LIM is merely capturing what would have been obtained from a simpler regression model on an ENSO index, perhaps also including some local ocean memory analogous to the "reddened ENSO" model of the Pacific Decadal Oscillation (Newman, Compo, & Alexander, 2003). Such a simple bivariate model (see Supporting Information S1 for details) does serve as a somewhat better baseline than damped persistence, but still exhibits considerably less skill compared to the LIM (cf. Figures S3 and S4 in Supporting Information S1 with Figures 3 and 4), demonstrating the importance of using the LIM's multivariate approach to capture spatially- and temporally-varying responses in the North Pacific to forcing by evolving ENSO events (Zhao et al., 2021).

3.3. Dependence of BTA Hindcast Skill on Bathymetric Depth

We next evaluate how BTA hindcast skill varies as a function of bathymetry depth and lead time (Figures 5a–5c), obtained by partitioning the range of bathymetric depths into 20 m bins, with hindcast skill averaged over each depth bin and lead time. This calculation is repeated separately for each sub-region.

Overall, hindcasts tend to be least skillful at locations with either the shallowest or deepest bottom depths, and have maximum skill when the bottom depth lies at ~50–150 m, depending upon latitude. For the southern sub-region at the shallowest depth bin, hindcast skill decreases rapidly with increasing lead time (Figure 5a). However, as the bottom depth increases to ~100 m, skill extends to longer lead times, still exceeding ~0.6 at 7-month lead. Below 100 m, skill again decreases more rapidly with lead time, an effect that intensifies with increasing depth. Similar results are seen for the other sub-regions (Figures 5b and 5c), although the northern sub-region is generally more skillful than the central sub-region across almost all bottom depths, and more skillful than the southern sub-region for leads greater than about 6 months.

By comparing hindcast skill to the forecast signal-to-noise ratios (Section 2.3; Figures 5d–5f), we find that the local variations in hindcast skill (Figures 5a–5c) reflect variations in regional and depth-dependent predictability, rather than occurring by chance. In all three sub-regions, the signal-to-noise ratio first increases with increasing bathymetry depth, and then gradually decreases, tracking the depth dependence of BTA forecast skill at all latitudes (cf. Figures 5d–5f with Figures 5a–5c). In the southern sub-region, the depth dependence of the signal-to-noise ratio and total variance (cf. Figure 5d with Figure 6) are generally similar, whereas, for the other two sub-regions, BTA

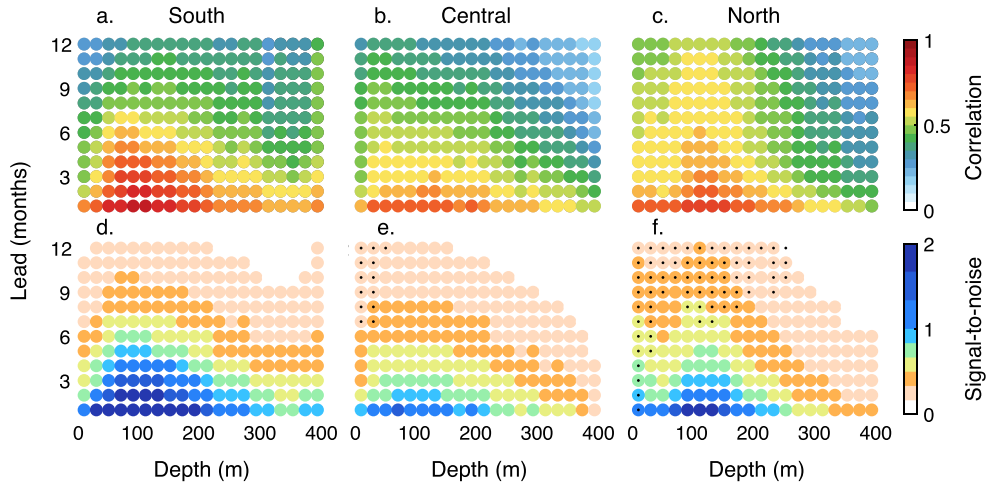

Figure 5. BTA (a–c) hindcast skill (anomaly correlation) and (d–f) signal-to-noise ratio, as a function of bathymetry depth and lead time. Each metric is separately evaluated for (a, d) southern, (b, e) central, and (c, f) northern sub-regions. The bathymetry depth is on the *x*-axis. Lead time is shown on the *y*-axis. (e, f) Black dots denote signal-to-noise ratio at a certain depth and lead time is higher than its counterpart in panel (d).

variance decreases monotonically with increasing bottom depth (Figure 6). This contrast highlights the relatively higher predictability for bottom depths of ~50–150 m, and for the northern sub-region. That is, in the northern sub-region, although the BTA variance and its predictable portion are both small, the noise is smaller, resulting in a relatively large signal-to-noise ratio and prediction skill extending to longer lead times.

3.4. Optimal BTA Evolution Linked to ENSO

To help diagnose the dynamics contributing to BTA prediction skill, we identify the 7-month-lead "optimal precursor," the initial conditions of coastal BTA, Pacific SSTA and SSHA that will most efficiently develop into large amplitude BTA after 7 months (Section 2.3). We then identify a subset (top 20%; i.e., 65 initial conditions out of the period 1993–2019) of the observed states that most strongly resemble this optimal precursor, and compare their subsequent observed composite evolution to that predicted by the LIM. (Here, "most strongly resemble" refers to the highest-ranking initial conditions based on their projections onto the identified optimal initial condition.) This also helps identify potential forecasts of opportunity (Section 2.3). The top 20% selected states consist of top 10% warm and top 10% cold samples. Cold samples are multiplied by −1 prior to deriving the composite.

The SSTA component of the observed initial condition for the resulting warm-minus-cold composite (shading of Figure 7a at 0-month lead) features warm anomalies in the central and eastern tropical Pacific and in the Northeast Pacific. Its observed composite evolution shows that tropical Pacific warm anomalies continue to strengthen through leads of about 6 months, and subsequently decay thereafter. Meanwhile, the initial SSHA component (contours in Figure 7a at 0-month lead) exhibits positive (negative) anomalies in the eastern (western) tropical Pacific. The amplitude of the east-west SSHA dipole structure in the tropical Pacific strengthens through leads of about 3 months, at about the point the equatorial Pacific zonal mean changes sign, and subsequently decays thereafter, leading the SST anomalies which is consistent with ENSO development.

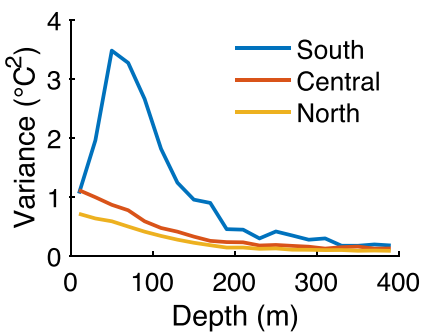

Figure 6. BTA variance as a function of bathymetry depth, separately evaluated for southern (blue), central (red), and northern (yellow) sub-regions.

The composite evolution of the observed BTA shows northward progression of the ENSO influence, with intensified BTA amplitudes occurring at longer lead time for higher latitudes (shading in Figure 7c). The observed BTA evolution is obtained by deriving the coastal spatial pattern for each lead time and taking a spatial average for each latitudinal bin (0.6° bin width, similar to

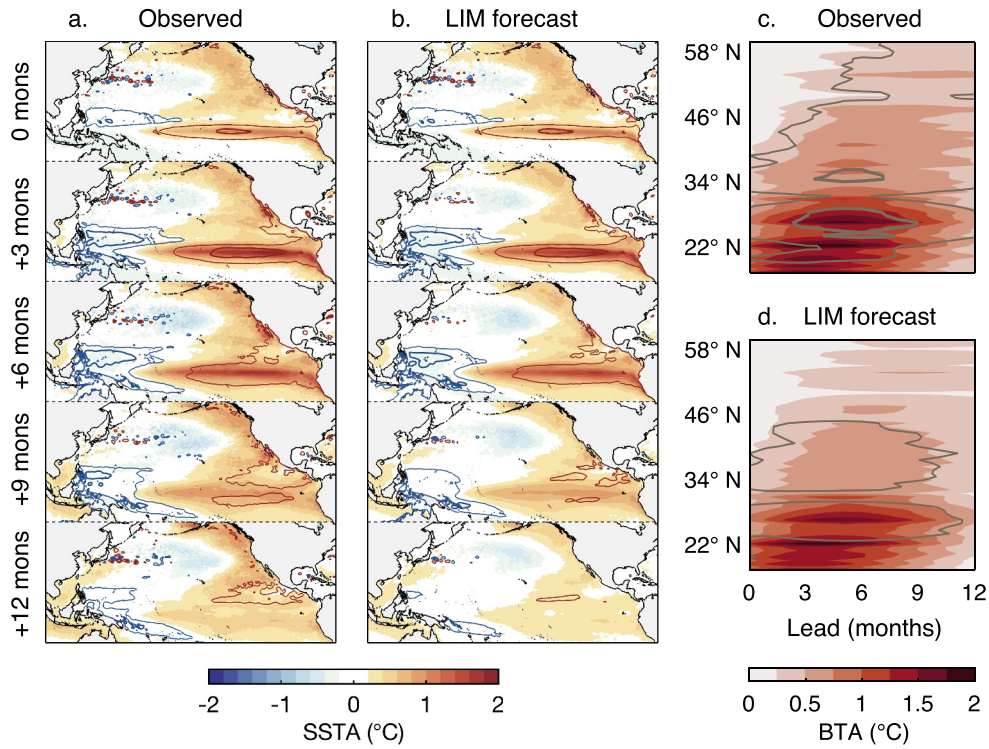

Figure 7. Forecast of opportunity identified by the optimal growth approach, and compared to observations (i.e., GLORYS12v1 reanalysis). (a, b) Lead 0 months shows the composite of the top 20% initial conditions that are most similar to the LIM's optimal precursor for coastal BTA. (a, b) Subsequent evolution at lead 3, 6, 9, 12 months is also composited, for (a) observations, and (b) LIM forecasts that are initialized from that top 20% conditions. Shading is SSTA. Contour is SSHA at 0.05 m (thin), 0.1 m (thick) (positive: red; negative: blue). (c, d) The top 20% initial BTA (shading) at 0 months and subsequent evolution at lead 1–24 months is composited, for (c) observation and (d) LIM forecast. Lead time is on *x*-axis. Latitude is on *y*-axis. The coastal SSTA is shown with contours at 0.6°C (thin), 1.2°C (thick).

the process of deriving Figure 2d), and is shown in a Hovmöller diagram. At 0-month lead, warm BTA is shown along the coastal domain, with stronger anomalies in the south and weaker in the north. As lead time increases, warm anomalies in the southern sub-region are gradually intensified, reaching a peak magnitude at ~3-to-6-month lead, and then decay, whereas in the northern part of the domain the peak magnitude occurs at a later lead time. Meanwhile, the coastal SSTA evolution is in phase with BTA (cf. contour with shading of Figure 7c). Together with the Pacific evolution shown in Figure 7a, these results suggest that the observed BTA amplification in the southern part of the domain coincides with ENSO development in the tropical Pacific, as both peak at the same lead time. For regions further away from the tropical Pacific, it takes a longer time for ENSO related influences to arrive and affect the local temperature variability, hence the delayed BTA amplification.

The result in Figure 7 is also largely representative of either warm or cold ENSO phases. To show this, we can separately analyze either the top 10% warm events (Figure 8a) or the top 10% cold events (Figure 8b). In both cases, although we have further reduced the sample sizes, results are similar to those obtained from the warm-minus-cold composite: The analysis based on the top 10% warm (cold) conditions links the positive (negative) BTA growth and forecast skill to the development of El Niño (La Niña) in the tropical Pacific (not shown), with a northward progression of the ENSO influence. Still, there is a noticeable difference between warm and cold composites in Figure 8: For increasing latitude, the peak BTA magnitude for the cold phase occurs at a lead time somewhat later than for the warm phase. This could reflect ENSO asymmetry and its varying influence on warm and cold BT evolutions. It could also reflect the smaller sample size in separate warm and cold composites; note also that the LIM hindcast composites captures some of the observed differences since the initial conditions for the hindcasts are themselves not symmetric. This aspect, however, is beyond the scope of this study.

Lastly, Figures 7b and 7d show that our composite of the LIM hindcasts, where each initialization has a strong projection on the optimal initial condition, largely captures the observed composite's anomaly growth and

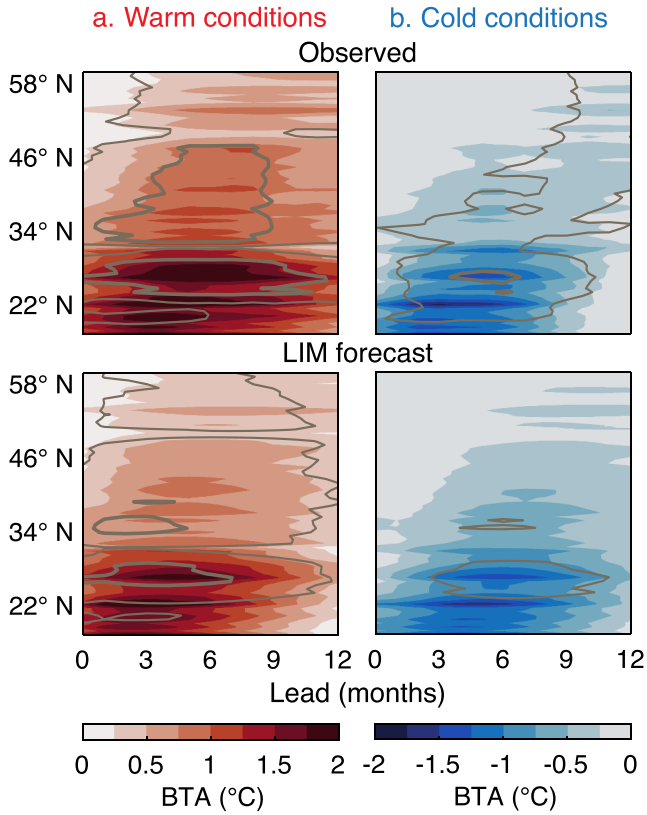

Figure 8. Same as Figures 7c and 7d except for the top 10% (a) warm conditions, (b) cold conditions.

evolution, although the predicted magnitude of the anomalies is somewhat underestimated at the longer lead times. More importantly, hindcasts whose initial conditions most resemble the optimal precursor have considerably elevated skill compared to the remaining hindcasts (Figure 9), suggesting that an initial high projection on the optimal precursor can be used to identify, a priori, the most skillful BTA forecasts.

4. Conclusions

In this study, using a LIM constructed from observed monthly Pacific SSTA, SSHA and coastal BTA, we investigated monthly BTA prediction along the North American West Coast for forecast leads of 1-to-12-month. The LIM's BTA hindcasts were considerably more skillful than damped persistence, with forecast skill (evaluated by anomaly correlation) exceeding 0.6 for much of the coastal region for lead times up to 6 months, and extending to even longer leads along the northernmost part of the coast. The season of maximum skill shifted from late fall to early spring from the southern to northern part of the coastal domain. Skill varied with bottom depth and was most pronounced at depths comparable to the depth of the thermocline along the North American West Coast, where variability can be large while the surface atmospheric noise is no longer felt, resulting in a higher signal-to-noise ratio of thermal anomalies at depth.

The LIM allowed us to identify, a priori, forecasts with high prediction skill arising from initial conditions with a large projection on the optimal precursors of BTA growth. These forecasts of opportunity are characterized by anomaly evolution consistent with ENSO development, implying that ENSO is a major contributor to BTA prediction skill beyond persistence. The delay in the timing of the maximum skill from south to north is consistent with the ENSO influence on the North American West Coast occurring through different mechanisms that operate at different lags. Poleward propagating coastally trapped waves originating on the equator have a stronger impact on the southern part of the domain, concurrent with or slightly lagging the development of ENSO events (e.g., Amaya et al., 2022; Engida et al., 2016; Jacox et al., 2015; Ray et al., 2020). In contrast, at higher latitudes, where the BT hindcast skill lags ENSO peak phase by several months, the ENSO influence may be more likely associated with atmospheric teleconnections into the North Pacific that peak a few months after the ENSO peak (Alexander et al., 2002; Deser & Blackmon, 1995; Zhao et al., 2021), which then force changes in the alongshore winds and consequently in coastal upwelling (Hermann et al., 2009; Jacox et al., 2015).

Notably, our LIM hindcast skill is qualitatively similar (M. G. Jacox, personal communication) to the dynamically downscaled forecasts over the period of 1982–2010 for the California Current System (Jacox et al., 2023), which were forced at the surface and the lateral ocean boundary by the outputs of the Canadian Center for Climate Modeling Analysis (Merryfield et al., 2013). Our finding of better hindcast skill for BTA at sites with relatively deeper depths than shallow depth locations is also consistent with J-SCOPE dynamical downscaling for Washington and Oregon coastal waters (Siedlecki et al., 2016), which targets a more localized domain with a more restricted time period of interests. Nonetheless, these dynamical downscaling models use very different bathymetry, leading to substantial differences in BTA along the coast (e.g., Amaya, Alexander, et al., 2023) and hence making a direct quantitative comparison between our LIM hindcasts and their results complicated and nontrivial.

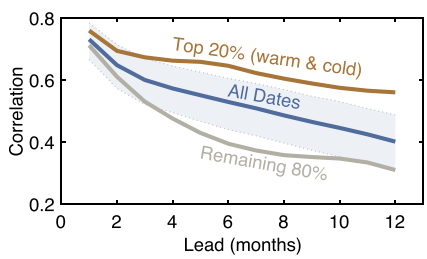

Figure 9. Skill of the hindcasts that are initialized from the top 20% initial conditions (brown), compared to skill of the remaining 80% hindcasts (gray), as well as hindcasts of all dates (blue). Skill is evaluated by spatially averaging the anomaly correlation within the coastal domain, for each lead. Blue shading represents the 95% confidence interval of the bootstrapped forecast skill.

In addition, the individual processes associated with ENSO and their relative roles in BTA forecasts are not explicitly examined in this study. However, the skillful BTA hindcasts and their dependence on season, bottom depth and

location imply that the LIM is capable of implicitly incorporating these effects. Nevertheless, the explicit representation of these processes through the inclusion of additional variables, such as thermocline depth, ocean currents or surface winds, in the construction of the LIM, may further improve BT forecasts and shed light on the relative roles of individual mechanisms. Moreover, while we emphasize the significant contribution from ENSO related dynamics, internal variability of the North Pacific could also play a role, which could be investigated in future studies by removing the tropical-extratropical coupling effect in the LIM (e.g., Zhao et al., 2021). Additionally, ENSO asymmetry (DiNezio & Deser, 2014; Martinez-Villalobos et al., 2019; Okumura & Deser, 2010; Wu et al., 2019) may influence warm and cold BT evolution and hindcasts differently. Addressing this aspect will require methodologies that can properly resolve asymmetric behaviors in the dynamical system, such as a LIM with state-dependent asymmetric noise (Martinez-Villalobos et al., 2019). All the above issues are intriguing topics that will be explored in future studies.

Data Availability Statement

GLORYS12v1 (Jean-Michel et al., 2021) reanalysis data are freely available at https://data.marine.copernicus.eu/product/GLOBAL_MULTIYEAR_PHY_001_030/services.

Acknowledgments
We gratefully acknowledge Dr. Michael G. Jacox for his valuable input and collaboration on the comparison of our LIM hindcasts with his dynamically downscaled forecasts for the California Current System (Jacox et al., 2023). T.X. was partly funded by the National Research Council (NRC) Research Associateship Programs. A.C. was supported by the NOAA Climate Program Office (CPO) Modeling, Analysis, Prediction and Projection (MAPP) Program. This work was supported by NOAA cooperative agreements NA17OAR4320101 and NA22OAR4320151.

References

Albers, J. R., & Newman, M. (2019). A priori identification of skillful extratropical subseasonal forecasts. *Geophysical Research Letters*, *46*(21), 12527–512536. https://doi.org/10.1029/2019gl085270

Alexander, M. A., Blade, I., Newman, M., Lanzante, J. R., Lau, N. C., & Scott, J. D. (2002). The atmospheric bridge: The influence of ENSO teleconnections on air-sea interaction over the global oceans. *Journal of Climate*, *15*(16), 2205–2231. https://doi.org/10.1175/1520-0442(2002)015<2205:tabtio>2.0.co;2

Alexander, M. A., Matrosova, L., Penland, C., Scott, J. D., & Chang, P. (2008). Forecasting Pacific SSTs: Linear inverse model predictions of the PDO. *Journal of Climate*, *21*(2), 385–402. https://doi.org/10.1175/2007jcli1849.1

Alexander, M. A., Scott, J. D., Jacox, M. G., Deser, C., Amaya, D. J., Capotondi, A., & Phillips, A. S. (2023). A survey of coastal conditions around the continental US using a high-resolution ocean reanalysis. *Progress in Oceanography*, *216*, 103055. https://doi.org/10.1016/j.pocean.2023.103055

Amaya, D. J., Alexander, M. A., Scott, J. D., & Jacox, M. G. (2023). An evaluation of high-resolution ocean reanalyses in the California Current System. *Progress in Oceanography*, *210*, 102951. https://doi.org/10.1016/j.pocean.2022.102951

Amaya, D. J., Jacox, M. G., Alexander, M. A., Scott, J. D., Deser, C., Capotondi, A., & Phillips, A. S. (2023). Bottom marine heatwaves along the continental shelves of North America. *Nature Communications*, *14*(1), 1038. https://doi.org/10.1038/s41467-023-36567-0

Amaya, D. J., Jacox, M. G., Dias, J., Alexander, M. A., Karnauskas, K. B., Scott, J. D., & Gehne, M. (2022). Subseasonal-to-Seasonal forecast skill in the California Current System and its connection to coastal Kelvin waves. *Journal of Geophysical Research: Oceans*, *127*(1), e2021JC017892. https://doi.org/10.1029/2021jc017892

Barbeaux, S. J., Holsman, K., & Zador, S. (2020). Marine heatwave stress test of ecosystem-based fisheries management in the Gulf of Alaska Pacific cod fishery. *Frontiers in Marine Science*, *7*, 703. https://doi.org/10.3389/fmars.2020.00703

Breaker, L. C. (2019). Long-range persistence in sea surface temperature off the coast of central California. *Journal of Ocean and Climate*, *9*, 1759313118791113. https://doi.org/10.1177/1759313118791113

Breeden, M. L., Albers, J. R., Butler, A. H., & Newman, M. (2022). The spring minimum in Subseasonal 2-m temperature forecast skill over north America. *Monthly Weather Review*, *150*(10), 2617–2628. https://doi.org/10.1175/mwr-d-22-0062.1

Breeden, M. L., Hoover, B. T., Newman, M., & Vimont, D. J. (2020). Optimal North Pacific blocking precursors and their deterministic subseasonal evolution during boreal winter. *Monthly Weather Review*, *148*(2), 739–761. https://doi.org/10.1175/mwr-d-19-0273.1

Cai, C., Kwon, Y.-O., Chen, Z., & Fratantoni, P. (2021). Mixed layer depth climatology over the northeast US continental shelf (1993–2018). *Continental Shelf Research*, *231*, 104611. https://doi.org/10.1016/j.csr.2021.104611

Capone, D. G., & Hutchins, D. A. (2013). Microbial biogeochemistry of coastal upwelling regimes in a changing ocean. *Nature Geoscience*, *6*(9), 711–717. https://doi.org/10.1038/ngeo1916

Capotondi, A., Deser, C., Phillips, A. S., Okumura, Y., & Larson, S. M. (2020). ENSO and Pacific decadal variability in the community Earth system model Version 2. *Journal of Advances in Modeling Earth Systems*, *12*, e2019MS002022. https://doi.org/10.1029/2019ms002022

Capotondi, A., Jacox, M., Bowler, C., Kavanaugh, M., Lehodey, P., Barrie, D., et al. (2019). Observational needs supporting marine ecosystems modeling and forecasting: From the global ocean to regional and coastal systems. *Frontiers in Marine Science*, *6*. https://doi.org/10.3389/fmars.2019.00623

Capotondi, A., Newman, M., Xu, T., & Di Lorenzo, E. (2022). An optimal precursor of northeast Pacific marine heatwaves and central Pacific El Niño events. *Geophysical Research Letters*, *49*(5), e2021GL097350. https://doi.org/10.1029/2021gl097350

Capotondi, A., Sardeshmukh, P. D., Di Lorenzo, E., Subramanian, A. C., & Miller, A. J. (2019). Predictability of US West Coast ocean temperatures is not solely due to ENSO. *Scientific Reports*, *9*(1), 10. https://doi.org/10.1038/s41598-019-47400-4

Castillo-Trujillo, A. C., Kwon, Y.-O., Fratantoni, P., Chen, K., Seo, H., Alexander, M. A., & Saba, V. S. (2023). An evaluation of eight global ocean reanalyses for the Northeast U.S. Continental shelf. *Progress in Oceanography*, *219*, 103126. https://doi.org/10.1016/j.pocean.2023.103126

Chen, Z., Kwon, Y., Chen, K., Fratantoni, P., Gawarkiewicz, G., Joyce, T. M., et al. (2021). Seasonal prediction of bottom temperature on the Northeast U.S. Continental shelf. *Journal of Geophysical Research: Oceans*, *126*(5), e2021JC017187. https://doi.org/10.1029/2021jc017187

Chi, L., Wolfe, C. L. P., & Hameed, S. (2018). Intercomparison of the Gulf Stream in ocean reanalyses: 1993–2010. *Ocean Modelling*, *125*, 1–21. https://doi.org/10.1016/j.ocemod.2018.02.008

Deser, C., & Blackmon, M. L. (1995). On the relationship between tropical and North Pacific Sea Surface temperature variations. *Journal of Climate*, *8*(6), 1677–1680. https://doi.org/10.1175/1520-0442(1995)008<1677:otrbta>2.0.co;2

DiNezio, P. N., & Deser, C. (2014). Nonlinear controls on the persistence of La Niña. *Journal of Climate*, *27*(19), 7335–7355. https://doi.org/10.1175/jcli-d-14-00033.1

Ding, H., Alexander, M. A., & Jacox, M. G. (2021). Role of geostrophic currents in future changes of coastal upwelling in the California Current System. *Geophysical Research Letters*, *48*(3), e2020GL090768. https://doi.org/10.1029/2020gl090768

Drinkwater, K. F., Beaugrand, G., Kaeriyama, M., Kim, S., Ottersen, G., Perry, R. I., et al. (2010). On the processes linking climate to ecosystem changes. *Journal of Marine Systems*, *79*(3–4), 374–388. https://doi.org/10.1016/j.jmarsys.2008.12.014

Engida, Z., Monahan, A., Ianson, D., & Thomson, R. E. (2016). Remote forcing of subsurface currents and temperatures near the northern limit of the California Current System. *Journal of Geophysical Research: Oceans*, *121*(10), 7244–7262. https://doi.org/10.1002/2016jc011880

Farrell, B. (1988). Optimal excitation of neutral Rossby waves. *Journal of the Atmospheric Sciences*, *45*(2), 163–172. https://doi.org/10.1175/1520-0469(1988)045<0163:oeonrw>2.0.co;2

Frankignoul, C., Gastineau, G., & Kwon, Y. O. (2017). Estimation of the SST response to anthropogenic and external forcing and its impact on the Atlantic multidecadal oscillation and the Pacific decadal oscillation. *Journal of Climate*, *30*(24), 9871–9895. https://doi.org/10.1175/jcli-d-17-0009.1

Frischknecht, M., Munnich, M., & Gruber, N. (2015). Remote versus local influence of ENSO on the California Current System. *Journal of Geophysical Research-Oceans*, *120*(2), 1353–1374. https://doi.org/10.1002/2014jc010531

Gómez-Valdivia, F., Parés-Sierra, A., & Laura Flores-Morales, A. (2017). Semiannual variability of the California undercurrent along the southern California Current System: A tropical generated phenomenon. *Journal of Geophysical Research: Oceans*, *122*(2), 1574–1589. https://doi.org/10.1002/2016jc012350

Hermann, A. J., Curchitser, E. N., Haidvogel, D. B., & Dobbins, E. L. (2009). A comparison of remote vs. local influence of El Niño on the coastal circulation of the northeast Pacific. *Deep Sea Research Part II: Topical Studies in Oceanography*, *56*(24), 2427–2443. https://doi.org/10.1016/j.dsr2.2009.02.005

Hervieux, G., Alexander, M. A., Stock, C. A., Jacox, M. G., Pegion, K., Becker, E., et al. (2019). More reliable coastal SST forecasts from the North American multimodel ensemble. *Climate Dynamics*, *53*(12), 7153–7168. https://doi.org/10.1007/s00382-017-3652-7

Jean-Michel, L., Eric, G., Romain, B.-B., Gilles, G., Angélique, M., Marie, D., et al. (2021). The Copernicus global 1/12 oceanic and sea ice GLORYS12 reanalysis. *Frontiers in Earth Science*, *9*. https://doi.org/10.3389/feart.2021.698876

Jacox, M. G., Alexander, M. A., Siedlecki, S., Chen, K., Kwon, Y. O., Brodie, S., et al. (2020). Seasonal-to-interannual prediction of North American coastal marine ecosystems: Forecast methods, mechanisms of predictability, and priority developments. *Progress in Oceanography*, *183*, 102307. https://doi.org/10.1016/j.pocean.2020.102307

Jacox, M. G., Alexander, M. A., Stock, C. A., & Hervieux, G. (2019). On the skill of seasonal sea surface temperature forecasts in the California Current System and its connection to ENSO variability. *Climate Dynamics*, *53*(12), 7519–7533. https://doi.org/10.1007/s00382-017-3608-y

Jacox, M. G., Buil, M. P., Brodie, S., Alexander, M. A., Amaya, D. J., Bograd, S. J., et al. (2023). Downscaled seasonal forecasts for the California Current System: Skill assessment and prospects for living marine resource applications. *PLOS Climate*, *2*(10), e0000245. https://doi.org/10.1371/journal.pclm.0000245

Jacox, M. G., Fiechter, J., Moore, A. M., & Edwards, C. A. (2015). ENSO and the California Current coastal upwelling response. *Journal of Geophysical Research: Oceans*, *120*(3), 1691–1702. https://doi.org/10.1002/2014jc010650

Kearney, K. A., Alexander, M., Aydin, K., Cheng, W., Hermann, A. J., Hervieux, G., & Ortiz, I. (2021). Seasonal predictability of sea ice and bottom temperature across the eastern Bering Sea shelf. *Journal of Geophysical Research: Oceans*, *126*(11), e2021JC017545. https://doi.org/10.1029/2021jc017545

Keller, A. A., Ciannelli, L., Wakefield, W. W., Simon, V., Barth, J. A., & Pierce, S. D. (2015). Occurrence of demersal fishes in relation to near-bottom oxygen levels within the California Current large marine ecosystem. *Fisheries Oceanography*, *24*(2), 162–176. https://doi.org/10.1111/fog.12100

Kurczyn, J. A., Pérez-Brunius, P., López, M., Candela, J., Delgadillo-Hinojosa, F., & García-Mendoza, E. (2019). Water masses and ocean currents over the continental slope off northern Baja California. *Journal of Geophysical Research: Oceans*, *124*(4), 2803–2823. https://doi.org/10.1029/2018jc013962

Liu, Z. Y., & Alexander, M. (2007). Atmospheric bridge, oceanic tunnel, and global climatic teleconnections. *Reviews of Geophysics*, *45*(2). https://doi.org/10.1029/2005rg000172

Long, X., Shin, S.-I., & Newman, M. (2023). Statistical downscaling of seasonal forecasts of sea level anomalies for U.S. Coasts. *Geophysical Research Letters*, *50*(4), e2022GL100271. https://doi.org/10.1029/2022gl100271

Long, X., Widlansky, M. J., Spillman, C. M., Kumar, A., Balmaseda, M., Thompson, P. R., et al. (2021). Seasonal forecasting skill of sea-level anomalies in a multi-model prediction framework. *Journal of Geophysical Research: Oceans*, *126*(6), e2020JC017060. https://doi.org/10.1029/2020jc017060

Lorenz, E. N. (1963). Deterministic nonperiodic flow. *Journal of the Atmospheric Sciences*, *20*(2), 130–141. https://doi.org/10.1175/1520-0469(1963)020<0130:dnf>2.0.co;2

Lou, J., O'Kane, T. J., & Holbrook, N. J. (2021). A linear inverse model of tropical and south Pacific climate variability: Optimal structure and stochastic forcing. *Journal of Climate*, *34*(1), 143–155. https://doi.org/10.1175/jcli-d-19-0964.1

Mariotti, A., Baggett, C., Barnes, E. A., Becker, E., Butler, A., Collins, D. C., et al. (2020). Windows of opportunity for skillful forecasts subseasonal to seasonal and beyond. *Bulletin of the American Meteorological Society*, *101*(5), E608–E625. https://doi.org/10.1175/bams-d-18-0326.1

Martinez-Villalobos, C., Newman, M., Vimont, D. J., Penland, C., & Neelin, J. D. (2019). Observed El Nino-La Nina asymmetry in a linear model. *Geophysical Research Letters*, *46*(16), 9909–9919. https://doi.org/10.1029/2019gl082922

Meinen, C. S., & McPhaden, M. J. (2000). Observations of warm water volume changes in the equatorial Pacific and their relationship to El Niño and La Niña. *Journal of Climate*, *13*(20), 3551–3559. https://doi.org/10.1175/1520-0442(2000)013<3551:oowwvc>2.0.co;2

Merryfield, W. J., Lee, W. S., Boer, G. J., Kharin, V. V., Scinocca, J. F., Flato, G. M., et al. (2013). The Canadian seasonal to interannual prediction system. Part I: Models and initialization. *Monthly Weather Review*, *141*(8), 2910–2945. https://doi.org/10.1175/mwr-d-12-00216.1

Murphy, A. H., & Epstein, E. S. (1989). Skill scores and correlation coefficients in model verification. *Monthly Weather Review*, *117*(3), 572–582. https://doi.org/10.1175/1520-0493(1989)117<0572:ssacci>2.0.co;2

Newman, M., Compo, G. P., & Alexander, M. A. (2003). ENSO-forced variability of the Pacific decadal oscillation. *Journal of Climate*, *16*(23), 3853–3857. https://doi.org/10.1175/1520-0442(2003)016<3853:evotpd>2.0.co;2

Newman, M., & Sardeshmukh, P. D. (2017). Are we near the predictability limit of tropical Indo-Pacific sea surface temperatures? *Geophysical Research Letters*, *44*(16), 8520–8529. https://doi.org/10.1002/2017gl074088

Newman, M., Sardeshmukh, P. D., Winkler, C. R., & Whitaker, J. S. (2003). A study of subseasonal predictability. *Monthly Weather Review*, *131*(8), 1715–1732. https://doi.org/10.1175//2558.1

Norton, E. L., Siedlecki, S., Kaplan, I. C., Hermann, A. J., Fisher, J. L., Morgan, C. A., et al. (2020). The importance of environmental exposure history in forecasting Dungeness crab Megalopae occurrence using J-SCOPE, a high-resolution model for the US Pacific northwest. *Frontiers in Marine Science*, *7*. https://doi.org/10.3389/fmars.2020.00102

Okumura, Y. M., & Deser, C. (2010). Asymmetry in the duration of El Niño and La Niña. *Journal of Climate*, *23*(21), 5826–5843. https://doi.org/10.1175/2010jcli3592.1

Ottersen, G., Kim, S., Huse, G., Polovina, J. J., & Stenseth, N. C. (2010). Major pathways by which climate may force marine fish populations. *Journal of Marine Systems*, *79*(3–4), 343–360. https://doi.org/10.1016/j.jmarsys.2008.12.013

Penland, C., & Sardeshmukh, P. D. (1995). The optimal-growth of tropical sea-surface temperature anomalies. *Journal of Climate*, *8*, 1999–2024. https://doi.org/10.1175/1520-0442(1995)008<1999:togots>2.0.co;2

Qiu, B., Chen, S. M., Schneider, N., & Taguchi, B. (2014). A coupled decadal prediction of the dynamic state of the Kuroshio extension system. *Journal of Climate*, *27*(4), 1751–1764. https://doi.org/10.1175/jcli-d-13-00318.1

Ray, S., Siedlecki, S. A., Alexander, M. A., Bond, N. A., & Hermann, A. J. (2020). Drivers of subsurface temperature variability in the northern California current. *Journal of Geophysical Research: Oceans*, *125*(8), e2020JC016227. https://doi.org/10.1029/2020jc016227

Sampaio, E., & Rosa, R. (2020). Climate change, multiple stressors, and responses of marine biota. *Climate Action*, 264–275. https://doi.org/10.1007/978-3-319-95885-9_90

Sardeshmukh, P. D., Compo, G. P., & Penland, C. (2000). Changes of probability associated with El Niño. *Journal of Climate*, *13*(24), 4268–4286. https://doi.org/10.1175/1520-0442(2000)013<4268:copawe>2.0.co;2

Scaife, A. A., & Smith, D. (2018). A signal-to-noise paradox in climate science. *NPJ Climate and Atmospheric Science*, *1*, 28. https://doi.org/10.1038/s41612-018-0038-4

Shin, S. I., & Newman, M. (2021). Seasonal predictability of global and North American coastal sea surface temperature and Height anomalies. *Geophysical Research Letters*, *48*(10). https://doi.org/10.1029/2020gl091886

Siedlecki, S. A., Kaplan, I. C., Hermann, A. J., Nguyen, T. T., Bond, N. A., Newton, J. A., et al. (2016). Experiments with seasonal forecasts of ocean conditions for the northern region of the California Current upwelling system. *Scientific Reports*, *6*(1), 27203. https://doi.org/10.1038/srep27203

Siegert, S., Bellprat, O., Ménégoz, M., Stephenson, D. B., & Doblas-Reyes, F. J. (2017). Detecting improvements in forecast correlation skill: Statistical testing and power analysis. *Monthly Weather Review*, *145*(2), 437–450. https://doi.org/10.1175/mwr-d-16-0037.1

Stock, C. A., Alexander, M. A., Bond, N. A., Brander, K. M., Cheung, W. W., Curchitser, E. N., et al. (2011). On the use of IPCC-class models to assess the impact of climate on living marine resources. *Progress in Oceanography*, *88*(1–4), 1–27. https://doi.org/10.1016/j.pocean.2010.09.001

Stock, C. A., Pegion, K., Vecchi, G. A., Alexander, M. A., Tommasi, D., Bond, N. A., et al. (2015). Seasonal sea surface temperature anomaly prediction for coastal ecosystems. *Progress in Oceanography*, *137*, 219–236. https://doi.org/10.1016/j.pocean.2015.06.007

Szekely, T., Gourrion, J., Pouliquen, S., & Reverdin, G. (2019). The CORA 5.2 dataset for global in situ temperature and salinity measurements: Data description and validation. *Ocean Science*, *15*(6), 1601–1614. https://doi.org/10.5194/os-15-1601-2019

Wen, C., Xue, Y., & Kumar, A. (2012). Seasonal prediction of North Pacific SSTs and PDO in the NCEP CFS hindcasts. *Journal of Climate*, *25*(17), 5689–5710. https://doi.org/10.1175/jcli-d-11-00556.1

Wu, X., Okumura, Y. M., & DiNezio, P. N. (2019). What controls the duration of El Niño and La Niña events? *Journal of Climate*, *32*(18), 5941–5965. https://doi.org/10.1175/jcli-d-18-0681.1

Xu, T., Newman, M., Capotondi, A., & Di Lorenzo, E. (2021). The continuum of northeast Pacific marine heatwaves and their relationship to the tropical Pacific. *Geophysical Research Letters*, *48*(2), 2020GL090661. https://doi.org/10.1029/2020gl090661

Xu, T., Newman, M., Capotondi, A., Stevenson, S., Di Lorenzo, E., & Alexander, M. A. (2022). An increase in marine heatwaves without significant changes in surface ocean temperature variability. *Nature Communications*, *13*(1), 7396. https://doi.org/10.1038/s41467-022-34934-x

Yang, X., Delworth, T. L., Zeng, F., Zhang, L., Cooke, W. F., Harrison, M. J., et al. (2021). On the development of GFDL's decadal prediction system: Initialization approaches and retrospective forecast assessment. *Journal of Advances in Modeling Earth Systems*, *13*(11), e2021MS002529. https://doi.org/10.1029/2021ms002529

Zhao, Y., Newman, M., Capotondi, A., Di Lorenzo, E., & Sun, D. (2021). Removing the effects of tropical dynamics from North Pacific climate variability. *Journal of Climate*, 1–49. https://doi.org/10.1175/jcli-d-21-0344.1